Atomic-spring-like effect in glassy silica-helium composites

Daniel T. Bowron, David A. Keen, Mathieu Kint, Coralie Weigel, Benoit Ruffle, Leszek Konczewicz, Sylvie Contreras, Benoit Coasne, Gaston Garbarino, Mickael Beaudhuin, Julien Haines, Jérôme Rouquette

Atomic-Spring-like Effect in Glassy silica-Helium Composites

Daniel T. Bowron*, David A. Keen*, Mathieu Kint, Coralie Weigel, Benoit Ruffle, Leszek Konczewicz, Sylvie Contreras, Benoit Coasne, Gaston Garbarino, Mickael Beaudhuin, Julien Haines, Jérôme Rouquette*

ISIS Facility, Rutherford Appleton Laboratory, Harwell Campus, Didcot, OX11 0QX, UK

L2C, Univ Montpellier, CNRS, Montpellier, France

Institut of High Pressure Physics, Polish Academy of Sciences, Sokołowska 29/37, 01-142 Warsaw, Poland.

Univ. Grenoble Alpes, CNRS, LIPhy, 38000 Grenoble, France

ESRF, 38000 Grenoble, France

ICGM, Univ Montpellier, CNRS, ENSCM, Montpellier, France

Email: Jerome.Rouquette@umontpellier.fr

Abstract

We determine the structural origin of an "atomic-spring-like effect" in a glassy silica-helium composite, which exhibits this mechanical property that reversibly accumulates and restores energy at the subnanoscale based on a high-pressure experimental pair distribution function study combined with atom-scale molecular simulations. These unexpected experimental results were obtained by using a 3 µm-spot size-61 keV X-ray beam and large area detector and by subtracting the scattered intensity due to helium

1

outside the sample from the silica signal at the same focal point for each pressure point. The compression behaviour of the glassy silica-helium composite is characterized on a structural level by the change from a uni-to-bi-modal distribution in the inter-tetrahedral distances in the amorphous isotropic structure of silica. We propose a simple characterization of this atomic-spring-like glass property using impedance spectroscopy measurements.

INTRODUCTION

Amorphous materials are structurally complex elements or compounds, some of which exhibit network glass topologies, with on-going fundamental questions on their local [1,2]/intermediate[3,4] orders, transitions between 'polyamorphs'[5,6] or in the liquid state [7,8]. These features, which are responsible for interesting physical properties, are widely used in optical and electronic devices as found in the special case of the archetype glassy silica, *g*-silica. The pair distribution function method is the technique of choice to resolve the structural correlations in these materials, but its application to high pressure studies has to date been limited due to the difficulty of accessing sufficient momentum transfer

for the scattered radiation when using diamond anvil cells. In this study, we have been able to overcome many of the issues that have limited previous work, and have obtained accurate x-ray structure factors up to $Q = 22.5$ Å^{-1}. This new capability has allowed us to obtain evidence of a novel structural mechanism that we have associated with an atomic-spring-like effect in the g-silica$-$He composite. An atomic-spring could be used in subnanoscale devices and sensors to measure "nano" forces and would offer an outstanding energy dissipation mechanism. The g-silica-He composite does not, at first glance, appear as an appropriate candidate for such an issue as g-silica is not defined as a porous material and only 0.0084 mol/cm^3/GPa of He were found to be inserted in g-silica at pressures up to 0.13 GPa [9]. However, g-SiO$_2$ exhibits a corner-sharing SiO$_4$ tetrahedra local structure which forms voids of n-fold rings (with $n \geq 2$, in g-SiO$_2$ mostly $n = 4, 5, 6, 7, 8$) [1,3,10-12], the radius of which is large enough for He (r_{He}=1.3 Å) to be inserted under pressure in the most common six-membered units [13], ($r_{6\text{-fold ring}}$ =1.5 Å). This scenario was confirmed and up to 1 mole of He could be inserted experimentally [14-16] (0.53 mole theoretically)[17] in g-silica under pressure. Interestingly, He as a pressurization fluid can be considered as a penetrating medium, whereas Ar atoms (r_{Ar}=1.88 Å), cannot be inserted so that pressurization using this fluid results in the normal densification of the material under compression. So far, the mechanism of helium

insertion has never been determined, so to gain insight we performed an *in situ* structural

investigation of helium insertion in *g*-silica at the beamline ID27 of the European

Synchrotron Radiation Facility (ESRF) based on a high-pressure X-ray pair distribution

function study (HP-PDF).

RESULTS AND DISCUSSION

High-quality PDFs require high-energy photons and access to large scattering angles to

measure data to high values of momentum transfer ($Q = 4\pi \sin \theta/\lambda$) [1,12,18]. In addition,

in order to obtain reliable HP-PDF, Bragg and Compton scattering from the diamond

anvils have to be removed. These surprising experimental results were made possible by

using a large area detector and by subtracting the scattered intensity of the 3 µm-spot size-

61 keV X-ray beam due to helium from the *g*-silica signal at the same focal point [19] for

each pressure point (Figure S1). The raw detector image data are shown, Figure S2, whilst

reduced and corrected data at *Patm* and 8.8 GPa used for structural modelling are shown

in Figure 1. The X-ray structure factor of *g*-silica obtained at *Patm* in the diamond cell up

to $Q = 22.5$ Å^{-1} along with the structure factor calculated from an empirical potential

structure refinement (EPSR) model [20,21] are shown on Figure 1.

The EPSR procedure generates an atomistic structural model subject to more than the

singular constraint of "fitting" the experimental data. Aside from matching the measured

structure factor, the model has to be consistent with the underpinning physical and

chemical requirements of system density and relative atomic sizes that govern the

distances of shortest approach that can be accommodated within the material. When

modelling a covalent glass such as silica, the EPSR procedure also uses Coulomb

interactions between silicon and oxygen sites to maintain the local chemical stoichiometry of the network, where the silicon atoms are assigned an effective charge of +4, and each oxygen atom a charge of -2 units. Collectively, these underpinning constraints limit how the atom-pair structural correlations can be accommodated in the model, and consequently mean that the refined structure will be unable to perfectly match the experimental data if they include systematic errors that are inconsistent with these fundamental criteria. As such, EPSR is a more robust mechanism to extract structural information from challenging experimental data than a direct rationalisation based on simply performing a Fourier transform of the measured structure factor to obtain a PDF assuming that the data have been perfectly collected and normalised. The analysis framework is in essence ensuring that the models are structural configurations that are consistent with both the measured structure factor and the a priori assumptions about the fundamental physical and chemical constraints that govern the system. Specifically, for the short-range interactions in *g*-silica, EPSR is only constrained by the Si-O bond length and the charge imposed requirement for silicon to be surrounded by oxygen atoms (and vice versa) in preference to directly bonded interactions of Si-Si and O-O type. At the pressures investigated, there is no reason to assume that the Si-O bond length would be shorter than the adopted 1.6Å average, found in bulk silica at STP, and so the refined models accommodate the pressure induced changes in the experimental structure factors through modifications to the angular correlations in the network and the second neighbour and longer pair correlations. The statistically best defined region of the experimental data, which dominates the refinement process, corresponds to the medium range network structure which is most subject to change in the pressure ranges investigated.

Upon increasing pressure, the first sharp peak of the X-ray structure factor of *g*-silica

decreases in intensity and broadens up to the highest pressure reached, Figure 1b (see also Figure S3). The comparison of the partial radial distribution functions obtained from the EPSR model with those simulated by molecular dynamics using the CHIK-potential [22] show very good agreement and are shown in Figure S4. This consistency between the two modelling approaches enhances our confidence that the local structure of g-silica derived by our atomistic structure refinement of the experimental scattering data is robust. In the EPSR structural model, the helium inserted values N_{He}^{P} at each pressure point were fixed to those determined using a poromechanical model relying on atom-scale Grand Canonical Monte Carlo simulations [17], see Figure S5. The partial radial distribution functions for Si-Si, Si-O, O-He obtained from the EPSR model are shown on Figure 2a-c, respectively. These data provide a means of understanding the structural modifications induced by the helium insertion at high pressure. The pressure induced changes consist of: i) a broadening of the Si-Si distance distribution (inter-tetrahedral distances) between the first and second coordination shells (Figure 2a), which additionally results in the appearance of a new contribution, observed above 3 Å, in the Si-O RDF (Figure 2b), and ii) a decrease in the O-He distance distribution with increasing pressure, which becomes sharper as a result of helium confinement (Figure 2c). Based on the EPSR model, access to bond angle distributions was possible and the Si-O-Si distributions are shown in Figure 2d. This representation gives the probability of a given bond angle, $P(\theta_{Si-O-Si})$, and is corrected for solid angle sampling, where the number of angles available at an angle θ is proportional to $\sin \theta$[23,24]; the estimation of the mean bond angle values can be obtained as the sum of these probabilities $P(\theta_{Si-O-Si})$ is equal to 1, so the mean is simply the point where $\Sigma(P(\theta_{Si-O-Si}))$ is 50% (Figure S6). At $Patm$ the Si-O-Si angle was found to have a mean value of 164° that is in agreement with literature reports from first principles

calculations [25,26], PDF[18,27] and NMR studies [28]. As already observed in Figure 2a with the Si-Si distance distribution, increasing pressure results in a change from a uni- to a bi-modal Si-O-Si bond angle distribution with the mean value decreasing from 164° to 161° at the highest pressure reached.

The pressure dependence of the Si-Si, Si-O and O-He coordination numbers obtained from the EPSR model is shown on Figure S7. This can be compared with previous high pressure studies which did not use any pressure transmitting medium and which resulted in an observed densification of *g*-silica mainly characterized by an increase in the Si-O coordination number to 6 for pressure greater than 15 GPa[29]. As already mentioned based on our HP-PDF study, He-insertion prevents the collapse of the framework and the Si-Si, Si-O first coordination number stay similar in the investigated pressure range. It has to be noted however that experiments performed without pressure transmitting medium (PTM) introduces strain into the glass sample and changes the structure in a different way as pressure is not hydrostatic at all (huge deviatoric stress). Using a non-penetrating PTM would give the genuine control result of the scattering from an unfilled SiO_2 glass at the given pressures, but only if you could be sure that the non-penetrating PTM has been accurately subtracted in the analysis. All non-penetrating PTMs will have a higher scattering signal /absorption to that of the He PTM used here making them more difficult to subtract accurately. Therefore, our present data can only be reliably be compared with calculations[30,31].

In order to understand the change in the local structure of *g*-silica due to helium insertion characterized by HP-PDF, it is particularly interesting to note the structural consequences of compression/gas insertion in microporous silica. In siliceous zeolites, compression behaviour is generally associated with changes in inter-tetrahedral bridging angles in the

SiO$_2$ framework resulting in a strong increase in pore ellipticity [32]; such a mechanism can be blocked by gas insertion, which will fill pores and prevent pore collapse [33-35]. As previously mentioned, the local structure of *g*-silica is defined by corner-sharing SiO$_4$ tetrahedra forming *n*-fold rings. During He-insertion, He-atoms (r_{He}=1.3 Å) are small enough: i) to be inserted under pressure in the most common six-membered rings [13] ($r_{6\text{-fold ring}}$ =1.5 Å) and prevent collapse of the framework and ii) to induce a change from uni- to bi-modal distribution in the inter-tetrahedra distance, which could be considered as a local distortion of the ring as determined by this HP-PDF study. Compression behaviour of *g*-silica in He therefore induces a splitting in the Si-Si distance distribution (Figure2a) associated with the appearance of a new contribution in the Si-O pair correlations at approximately 3 Å (Figure2b) and induces a bimodal Si-O-Si bond angle distribution (Figure 2d) which is consistent with the pressure-induced local symmetry breaking reported by Shi and Tanaka[36]. Figure 3a schematically represents the mechanism of He-insertion in a six-membered rings, in which insertion of He-atoms acts as an atomic-spring-like preventing ring collapse and inducing a local distortion under compression. Note that the He-insertion induced appearance of a local distortion could not be predicted in the poromechanical model, as such a microscopic change in the local structure would require density functional theory calculations using a similar *g*-silica cell dimension as those of the models used here, which is not currently achievable [6].

In order to characterize He-insertion in *g*-silica, which is found to exhibit an atomic-spring-like effect as described above, Sato et al. previously reported microscopic observation of the system to estimate the equation of state of *g*-silica in a penetrating (He) and non-penetrating medium (methanol-ethanol)[14]. Later, Weigel et al. [37] used the

Clausius-Mossotti relationship to estimate the helium inserted values $N_{He}{}^{P}$ based on the measurement of the refractive index in g-silica, studied by Brillouin spectroscopy [38]. Due to the relationship between refractive index, dielectric permittivity and complex impedance, the spring glass properties of the g-silica-He composite can be determined by impedance spectroscopy (Figure S10). Figure 3b shows the pressure dependence of the relative impedance data (Z/Z_0) obtained for g-silica in a penetrating (He), i.e. atomic-spring-like, and non-penetrating medium (gasoline F) up to 1.6 GPa during compression/decompression. It is interesting to note first that both data exhibit an equation of state-like profile with Z/Z_0 values higher in He than those in gasoline. Data are perfectly reproducible under decompression and this is consistent with a reversible mechanism of He insertion/removal. Additionally, relative impedance values for a penetrating/non penetrating medium at the highest pressure reached, i.e. ~ 0.957/0.932, are in qualitative agreement with those reported for V/V_0 (~ 0.975/0.95); notably, the impedance difference value is similar to that of the volume difference between the two sets of data in a penetrating/non penetrating medium (~2.5%). Impedance spectroscopy measurements probe an absence of change in the electron density of state in g-silica within this pressure-range, which depends therefore only on the volume; this is why one can understand such similarities between Z/Z_0 and V/V_0 data. Note that estimated values

9

of the relative volume based on impedance measurement are probably more accurate than those estimated by microscopic observation due to a greater sensitivity and resolution.

CONCLUSIONS

The present study has determined the structural mechanism linked to He-insertion in *g*-silica based on an EPSR model, which was only possible with accurate high-pressure X-ray structure factors. The "atomic-spring mechanical property" should arise from the reversible elastic distortion of the glass network due to the presence of helium, mainly in six-membered rings of SiO_4 tetrahedra, under pressure. We have shown the reversibility of the behaviour in Figure 3c based on impedance spectroscopy measurements. This reversibility was already observed by Sato et al.[14], Weigel et al. based on Brillouin[37] and Raman spectroscopy measurements[39]. Admittedly this study does not provide X-ray PDF derived structural evidence of the associated elastic behaviour, and in light of this, perhaps the term "spring-like" would be a more appropriate description. As previously mentioned, from a poromechanical perspective, up to 0.5 mole of He can be inserted in the most common six-membered rings, both preventing the collapse of the ring due to atomic-spring-like effect and inducing a local distortion in the isotropic glass matrix. Such a composite can easily be achieved and characterized as shown by the present example of impedance spectroscopy measurements.

We expect that the present finding will stimulate further investigation in order to use such an effect in applications in sub-nanoscale devices and sensors which would enable to measure infinitesimal forces and would offer an exceptional energy dissipation mechanism. Such a strategy could potentially provide, for example, an interesting approach from the perspective of energy storage capacity.

Supporting Information

The Supporting Information describes the methods used in the present study

AUTHOR INFORMATION

Corresponding Author

* *Jérôme Rouquette* - ICGM, Univ Montpellier, CNRS, ENSCM, Montpellier, France ;
https://orcid.org/0000-0002-6880-1715

Email : Jerome.Rouquette@umontpellier.fr

Daniel T. Bowron - ISIS Facility, Rutherford Appleton Laboratory, Harwell Campus, Didcot, OX11 0QX, UK

; https://orcid.org/0000-0002-4557-1929

Email : daniel.bowron@stfc.ac.uk

David A. Keen - ISIS Facility, Rutherford Appleton Laboratory, Harwell Campus, Didcot, OX11 0QX, UK

https://orcid.org/0000-0003-0376-2767

Email : david.keen@stfc.ac.uk

Authors

Mathieu Kint - L2C, Univ Montpellier, CNRS, Montpellier, France

Email : mathieu.kint@hotmail.fr

Coralie Weigel *- L2C, Univ Montpellier, CNRS, Montpellier, France*

Email : Coralie.Weigel@umontpellier.fr

Benoit Ruffle *- L2C, Univ Montpellier, CNRS, Montpellier, France*

Email : Benoit.ruffle@umontpellier.fr

Leszek Konczewicz *- L2C, Univ Montpellier, CNRS, Montpellier, France ; Institut of High Pressure Physics, Polish Academy of Sciences, Sokołowska 29/37, 01-142 Warsaw, Poland.*

Email : leszek.konczewicz@umontpellier.fr

Sylvie Contreras *- L2C, Univ Montpellier, CNRS, Montpellier, France*

Email : Sylvie.Contreras@umontpellier.fr

Benoit Coasne *- Univ. Grenoble Alpes, CNRS, LIPhy, 38000 Grenoble, France*; https://orcid.org/0000-0002-3933-9744

Email : benoit.coasne@univ-grenoble-alpes.fr

Gaston Garbarino *- ESRF, 38000 Grenoble, France*; https://orcid.org/0000-0003-4780-9520

Email : gaston.garbarino@esrf.fr

Mickael Beaudhuin- ICGM, Univ Montpellier, CNRS, ENSCM, Montpellier, France

Email : Mickael.Beaudhuin@umontpellier.fr

Julien Haines - ICGM, Univ Montpellier, CNRS, ENSCM, Montpellier, *France ; https://orcid.org/0000-0002-7030-3213*
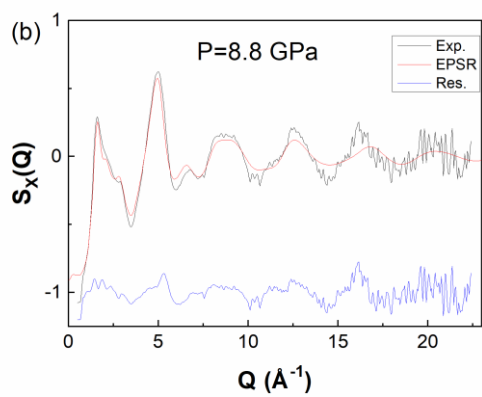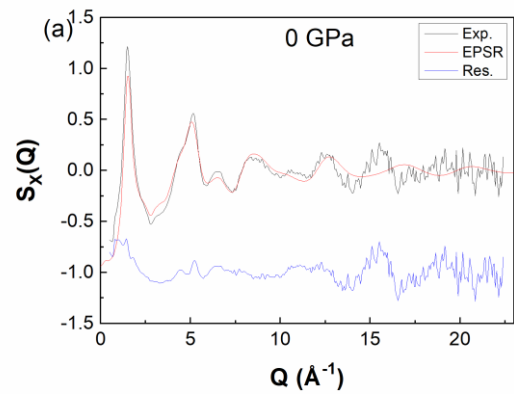
Email : Julien.Haines@umontpellier.fr

ACKNOWLEDGMENT

Figure 1. *g*-silica−He composite structure factor $S_X(Q)$ (black): (a), at *Patm*, (b), at 8.8 GPa; red and blue lines show calculated EPSR model and the difference between calculated and experimental data, respectively.
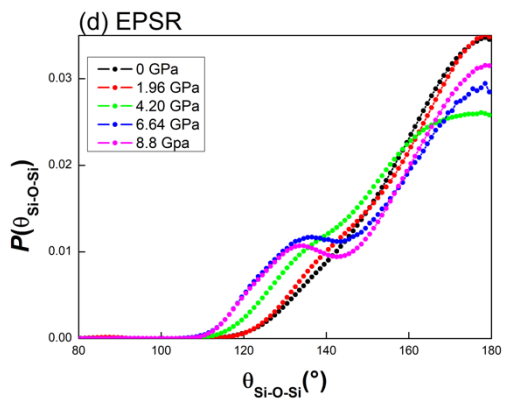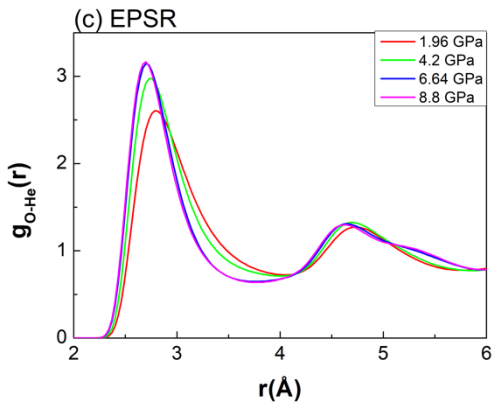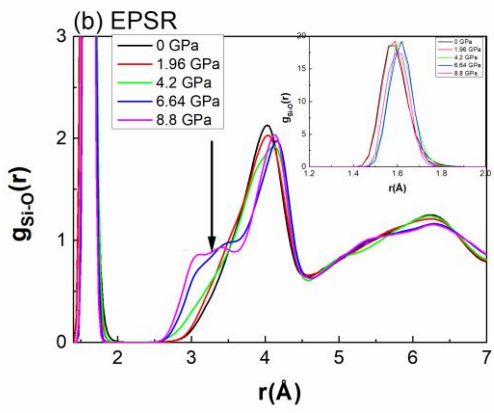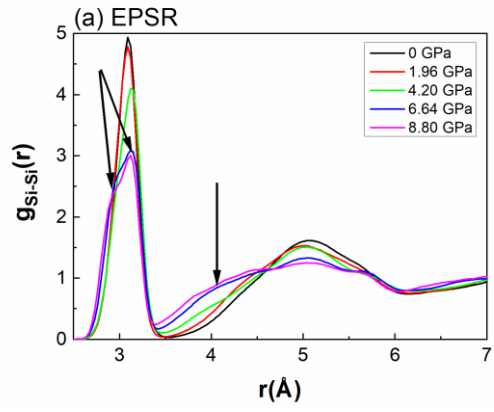
Figure 2. Pressure dependence of the partial radial distribution functions from EPSR model of g-silica-He composite: (a) $g_{Si\text{-}Si}(r)$, (b) $g_{Si\text{-}O}(r)$, (c) $g_{O\text{-}He}(r)$; arrows either show the appearance of a bi-modal distribution or of a new contribution, and (d) Pressure dependence of Si-O-Si bond angle distribution functions.
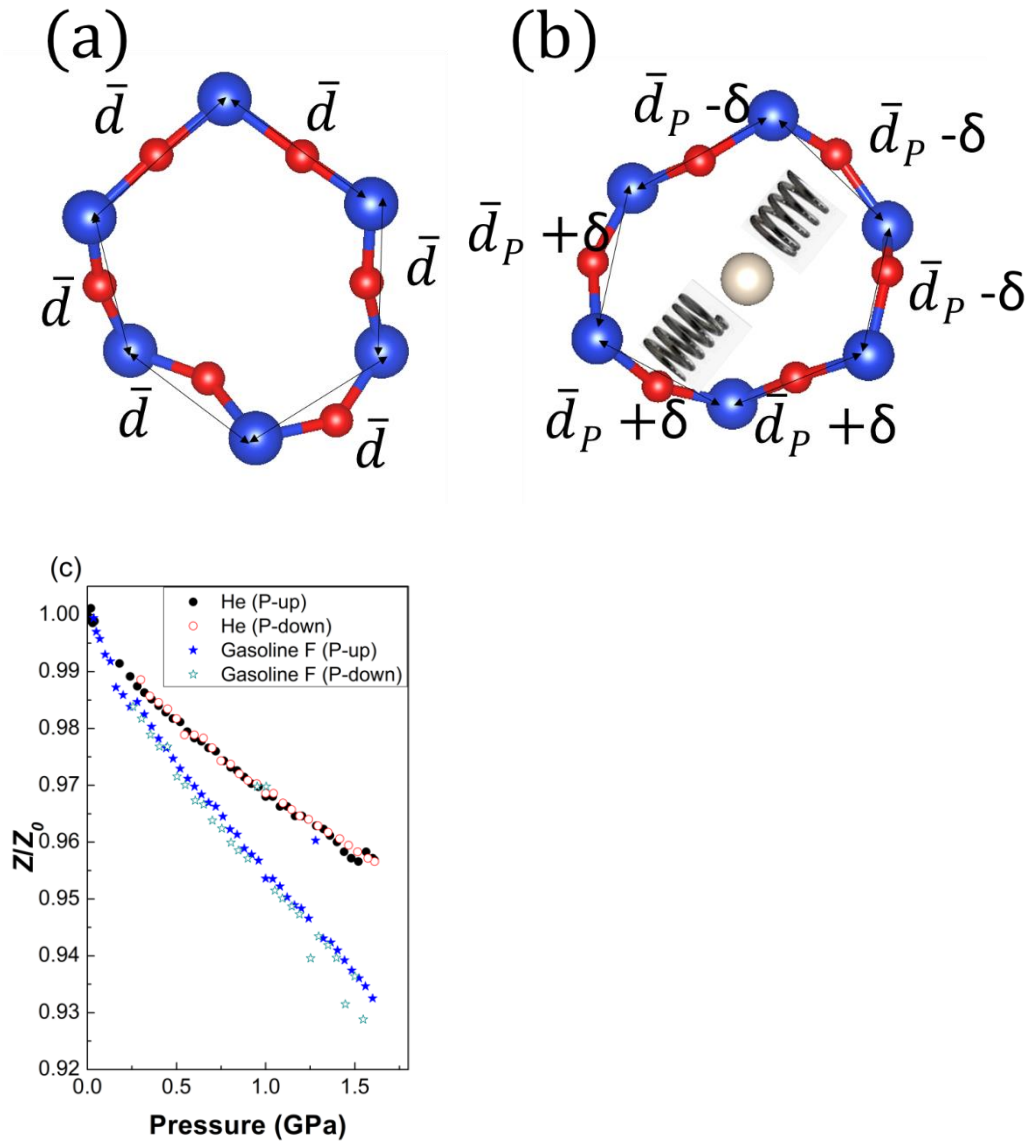
Figure 3. Atomic-spring-like effect in *g*-silica. Mechanism of He-insertion in an example of a six-membered rings obtained (a) at *Patm* and at (b) 8.8 GPa from PDF data, in which the presence of He-atoms acts as an atomic-spring preventing ring collapse and inducing uninomodal ($\bar{d}$)-to-bimodal ($\overline{d_P} + \delta$, $\overline{d_P}$-δ) distribution of the inter-tetrahedral distance; red, blue and white spheres represent Si and O and He atoms respectively (c) Pressure dependence of the relative impedance measurements (obtained at 2 MHz) of *g*-silica with a penetrating medium (He) and on a non-penetrating medium (Gasoline F).

17

For Table of Content Only
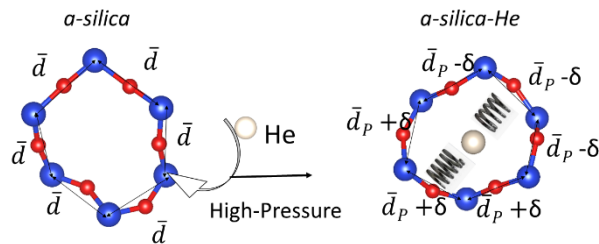
Graphic for Manuscript

References

1   Keen, D. A. & Dove, M. T. Local structures of amorphous and crystalline phases of silica, SiO(2), by neutron total scattering. *J. Phys.-Condes. Matter* **11**, 9263-9273, doi:10.1088/0953-8984/11/47/311 (1999).

2   Sheng, H. W., Luo, W. K., Alamgir, F. M., Bai, J. M. & Ma, E. Atomic packing and short-to-medium-range order in metallic glasses. *Nature* **439**, 419-425, doi:10.1038/nature04421 (2006).

3   Elliott, S. R. Medium-range structural order in covalent amorphous solids. *Nature* **354**, 445-452, doi:10.1038/354445a0 (1991).

4   Keen, D. A. & Goodwin, A. L. The crystallography of correlated disorder. *Nature* **521**, 303-309, doi:10.1038/nature14453 (2015).

5   Wilding, M. C., Wilson, M. & McMillan, P. F. Structural studies and polymorphism in amorphous solids and liquids at high pressure. *Chem. Soc. Rev.* **35**, 964-986, doi:10.1039/b517775h (2006).

6   Deringer, V. L. *et al.* Origins of structural and electronic transitions in disordered silicon. *Nature* **589**, 59-64, doi:10.1038/s41586-020-03072-z (2021).

7   Debenedetti, P. G., Sciortino, F. & Zerze, G. H. Second critical point in two

realistic models of water. *Science* **369**, 289-+, doi:10.1126/science.abb9796 (2020).

8   Henry, L. *et al.* Liquid-liquid transition and critical point in sulfur. *Nature* **584**, 382-+, doi:10.1038/s41586-020-2593-1 (2020).

9   Shelby, J. E. Pressure-dependence of Helium and Neon solubility in vitreous silica. *J. Appl. Phys.* **47**, 135-139, doi:10.1063/1.322359 (1976).

10   King, S. V. Ring configurations in a random network model of vitreous silica. *Nature* **213**, 1112-&, doi:10.1038/2131112a0 (1967).

11   Sarnthein, J., Pasquarello, A. & Car, R. structural and electronic-properties of liquid and amorphous SIO2 - an ab-initio molecular-dynamics study. *Phys. Rev. Lett.* **74**, 4682-4685, doi:10.1103/PhysRevLett.74.4682 (1995).

12   Tucker, M. G., Dove, M. T. & Keen, D. A. Application of the reverse Monte Carlo method to crystalline materials. *J. Appl. Crystallogr.* **34**, 630-638, doi:10.1107/s002188980100930x (2001).

13   Pasquarello, A. & Car, R. Identification of Raman defect lines as signatures of ring structures in vitreous silica. *Phys. Rev. Lett.* **80**, 5145-5147, doi:10.1103/PhysRevLett.80.5145 (1998).

14   Sato, T., Funamori, N. & Yagi, T. Helium penetrates into silica glass and reduces its compressibility. *Nat. Commun.* **2**, doi:10.1038/ncomms1343 (2011).

15   Shen, G. Y. *et al.* Effect of helium on structure and compression behavior of SiO2 glass. *P Natl Acad Sci USA* **108**, 6004-6007, doi:10.1073/pnas.1102361108 (2011).

16   Weigel, C. *et al.* Vitreous Silica Distends in Helium Gas: Acoustic Versus Static Compressibilities. *Phys. Rev. Lett.* **109**, doi:10.1103/PhysRevLett.109.245504 (2012).

17   Coasne, B. *et al.* Poroelastic Theory Applied to the Adsorption-Induced Deformation of Vitreous Silica. *J Phys Chem B* **118**, 14519-14525, doi:10.1021/jp5094383 (2014).

18   Tucker, M. G., Keen, D. A., Dove, M. T. & Trachenko, K. Refinement of the Si-O-Si bond angle distribution in vitreous silica. *J. Phys.-Condes. Matter* **17**, S67-S75, doi:10.1088/0953-8984/17/5/008 (2005).

19   Details are shown in SI

20   Soper, A. K. Partial structure factors from disordered materials diffraction data: An approach using empirical potential structure refinement. *Phys. Rev. B* **72**, doi:10.1103/PhysRevB.72.104204 (2005).

21   Bowron, D. T. An experimentally consistent atomistic structural model of silica glass. *Mater. Sci. Eng. B-Adv. Funct. Solid-State Mater.* **149**, 166-170, doi:10.1016/j.mseb.2007.11.030 (2008).

22   Carre, A., Horbach, J., Ispas, S. & Kob, W. New fitting scheme to obtain effective

potential from Car-Parrinello molecular-dynamics simulations: Application to silica. *Epl* **82**, doi:10.1209/0295-5075/82/17001 (2008).

23 Kroon, J. & Kanters, J. A. Non-linearity of hydrogen bonds in molecular crystals. *Nature* **248**, 667-669, doi:10.1038/248667a0 (1974).

24 Baur, W. H. Straight SI-O-SI bridging bonds do exist in silicates and silicon dioxide polymorphs. *Acta Crystallogr. Sect. B-Struct. Sci.Cryst. Eng. Mat.* **36**, 2198-2202, doi:10.1107/s0567740880008382 (1980).

25 Umari, P., Gonze, X. & Pasquarello, A. Concentration of Small Ring Structures in Vitreous Silica from a First-Principles Analysis of the Raman Spectrum. *Phys. Rev. Lett.* **90**, 027401, doi:10.1103/PhysRevLett.90.027401 (2003).

26 Giacomazzi, L., Umari, P. & Pasquarello, A. Medium-range structure of vitreous ${\text{SiO}}_{2}$ obtained through first-principles investigation of vibrational spectra. *Phys. Rev. B* **79**, 064202, doi:10.1103/PhysRevB.79.064202 (2009).

27 Kohara, S. & Suzuya, K. Intermediate-range order in vitreous SiO2and GeO2. *Journal of Physics: Condensed Matter* **17**, S77-S86, doi:10.1088/0953-8984/17/5/009 (2005).

28 Mauri, F., Pasquarello, A., Pfrommer, B. G., Yoon, Y.-G. & Louie, S. G. Si-O-Si bond-angle distribution in vitreous silica from first-principles ${}^{29}\mathrm{Si}$ NMR analysis. *Phys. Rev. B* **62**, R4786-R4789, doi:10.1103/PhysRevB.62.R4786 (2000).

29 Benmore, C. J. *et al.* Structural and topological changes in silica glass at pressure. *Phys. Rev. B* **81**, doi:10.1103/PhysRevB.81.054105 (2010).

30 Tse, J. S., Klug, D. D. & Lepage, Y. High-pressure densification of amorphous silica. *Phys. Rev. B* **46**, 5933-5938, doi:10.1103/PhysRevB.46.5933 (1992).

31 Hasmy, A., Ispas, S. & Hehlen, B. Percolation transitions in compressed SiO2 glasses. *Nature* **599**, 62-+, doi:10.1038/s41586-021-03918-0 (2021).

32 Thibaud, J. M. *et al.* High-Pressure Phase Transition, Pore Collapse, and Amorphization in the Siliceous 1D Zeolite, TON. *J. Phys. Chem. C* **121**, 4283-4292, doi:10.1021/acs.jpcc.6b11594 (2017).

33 Colligan, M. *et al.* Synchrotron X-ray powder diffraction and computational investigation of purely siliceous zeolite Y under pressure. *J. Am. Chem. Soc.* **126**, 12015-12022, doi:10.1021/ja048685g (2004).

34 Arletti, R. *et al.* Pressure-induced penetration of guest molecules in high-silica zeolites: the case of mordenite. *Phys Chem Chem Phys* **17**, 24262-24274, doi:10.1039/c5cp03561a (2015).

35 Thibaud, J. M. *et al.* Saturation, of the Siliceous Zeolite TON with Neon at High

Pressure. *J. Phys. Chem. C* **122**, 8455-8460, doi:10.1021/acs.jpcc.8b01827 (2018).

36   Shi, R. & Tanaka, H. Impact of local symmetry breaking on the physical properties of tetrahedral liquids. *P Natl Acad Sci USA* **115**, 1980-1985, doi:10.1073/pnas.1717233115 (2018).

37   Weigel, C. *et al.* Vitreous Silica Distends in Helium Gas: Acoustic Versus Static Compressibilities. *Phys. Rev. Lett.* **109**, 245504, doi:10.1103/PhysRevLett.109.245504 (2012).

38   Details are shown in SI

39   Weigel, C. *et al.* Polarized Raman spectroscopy of v-SiO2 under rare-gas compression. *Phys. Rev. B* **93**, doi:10.1103/PhysRevB.93.224303 (2016).

Supporting Information

Atomic-Spring-like Effect in Glassy silica-Helium Composites

Daniel T. Bowron*, David A. Keen*, Mathieu Kint, Coralie Weigel, Benoit Ruffle, Leszek Konczewicz, Sylvie Contreras, Benoit Coasne, Gaston Garbarino, Mickael Beaudhuin, Julien Haines, Jérôme Rouquette*

ISIS Facility, Rutherford Appleton Laboratory, Harwell Campus, Didcot, OX11 0QX, UK

L2C, Univ Montpellier, CNRS, Montpellier, France

Institut of High Pressure Physics, Polish Academy of Sciences, Sokołowska 29/37, 01-142 Warsaw, Poland.

Univ. Grenoble Alpes, CNRS, LIPhy, 38000 Grenoble, France

ESRF, 38000 Grenoble, France

ICGM, Univ Montpellier, CNRS, ENSCM, Montpellier, France

Email: Jerome.Rouquette@umontpellier.fr

Methods

High-Pressure Pair Distribution Function Study

The *g*-silica sample consists of a 54 µm thick Suprasil F300 platelet containing less than 1ppm OH (Heraeus Quartzglass, Germany), which was measured as a function of pressure up to 8.8 GPa using a diamond anvil cell (DAC) at room temperature with a helium pressure transmitting medium and a ruby sphere to measure pressure calibration[1], Figure S1(left). Scattering Geometry of the HP-PDF study, Figure S1(right), is also shown in order to identify the constrained geometry using a DAC governed by the opening angle of the diamonds and their backing discs. In this experiment Boehler-Almax 80° (4θ)- large aperture angle diamonds were specifically used to access sufficient momentum transfer for the scattered radiation.

An X-ray energy of 61keV and a Perkin-Elmer flat panel large area detector was used on the ID27 instrument at the ESRF.
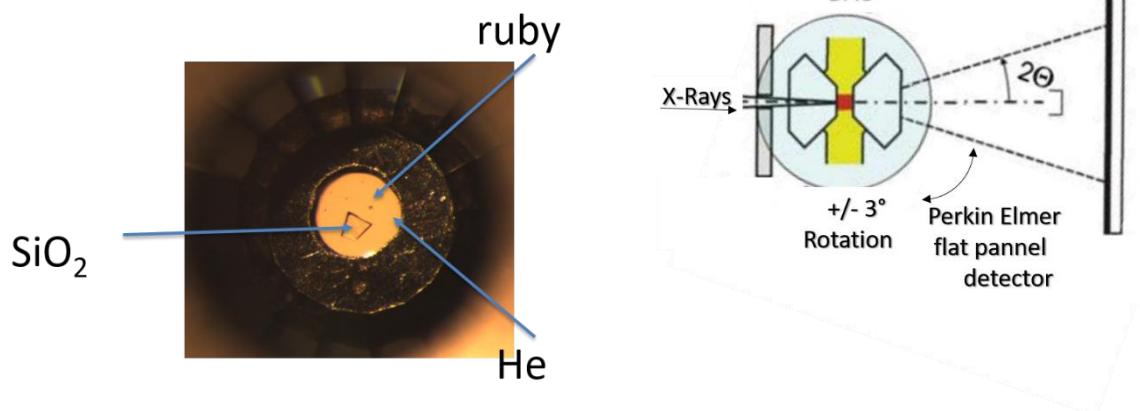
Figure S1. (left) *g*-silica-He loaded DAC. *g*-silica, ruby sphere and He are shown. (right) Scattering geometry of the HP-PDF study.

We used Fit2D to mask the diamond Bragg spots and other obvious spurious aberrations in the data for the X-ray beam passing through the DAC and the sample (Fig S2(a)) and offset from the sample (Fig S2 (b)) as a background. It was then used to generate the scattering as a function of (azimuthally averaged) 2θ for each dataset. These data were then normalised using GudrunX[2].

We emphasise that the diamond Bragg spots were removed by generously masking out those regions on the detector where they occurred such that the background was largely featureless. A background measurement was taken at each pressure to account for any change of DAC geometry with pressure and the *same* mask was used for *all* datasets. The background subtraction will also remove the diamond Compton contribution.

Fit2D accounts for polarization and Gudrun accounts for absorption and multiple scattering of the sample. Sample absorption and multiple scattering were most likely very small and likely to be smoothly varying with 2θ and unlikely to contribute any 'features'. They might not be so small for the diamonds, but this would be the same for both measurements. Note that the difference plot, Figure S2c, exhibits non-concentric circles which arise from the shadowing of the various apertures in the set-up (gasket hole, backing discs etc.) and are the result of moving the DAC between the measurements in Figure S2(a) and Figure S2(b). Therefore, we only included the parts of the detector where the subtracted data were the cleanest (note that the mask

was the same for every measurement). In order to validate such a procedure, which could show some artifacts at high Q, the Empirical Potential Structure Refinement models below were run using the entire Q-range (to 22.5 Å^{-1}) and with a reduced Q-range up to 15 Å^{-1} applied to the input experimental data.
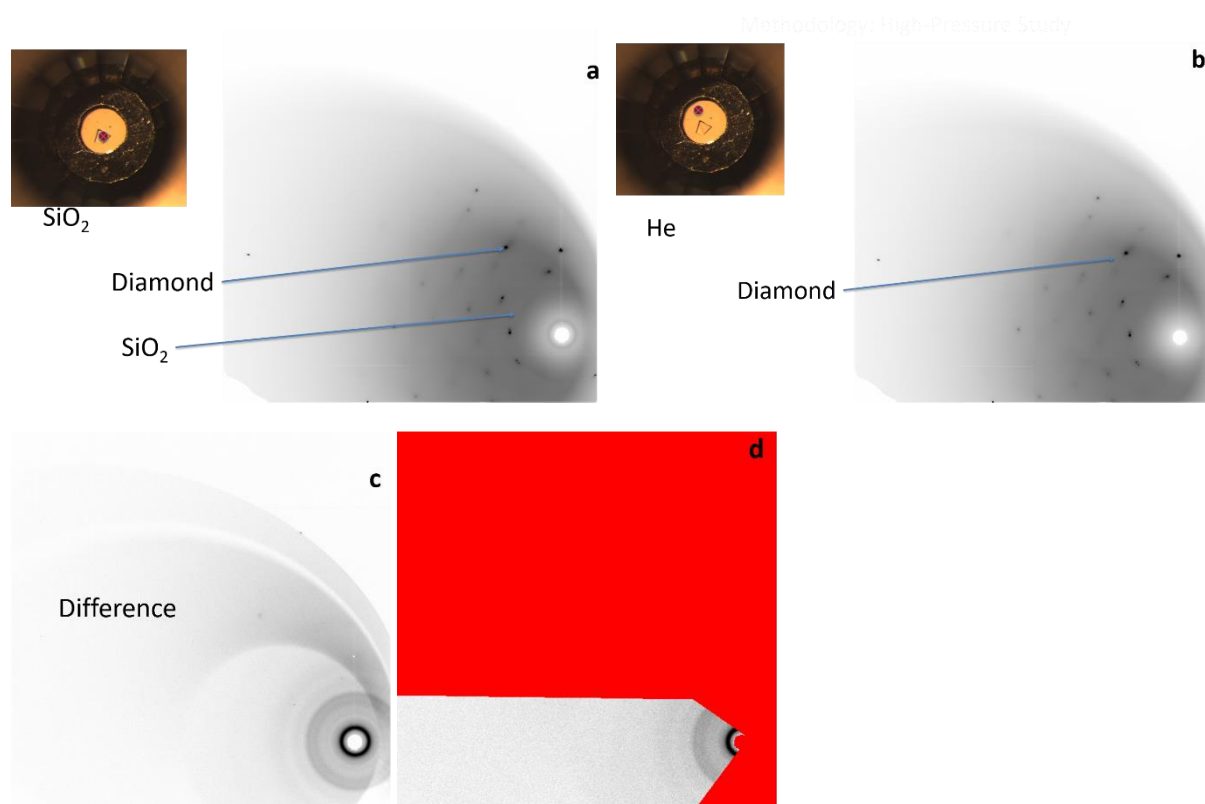

Figure S2. a-silica-He intensity profile of a 2-dimensional diffraction pattern of a 3 µm-spot size-61 KeV beam from (a), g-silica + Helium, (b) Helium, (c) difference, (d) intensity of the g-silica-He x-ray total scattering.

Empirical Potential Structure Refinement (EPSR)

EPSR uses a simple Lennard-Jones + Coulomb pair-wise potential to restrain the model, as well as the data. The L-J parameters were chosen to mimic the Van der Waals radii and were fixed at the same value for all pressures. The coulomb charges were +2 (Si), -1 (O) and 0 (He).
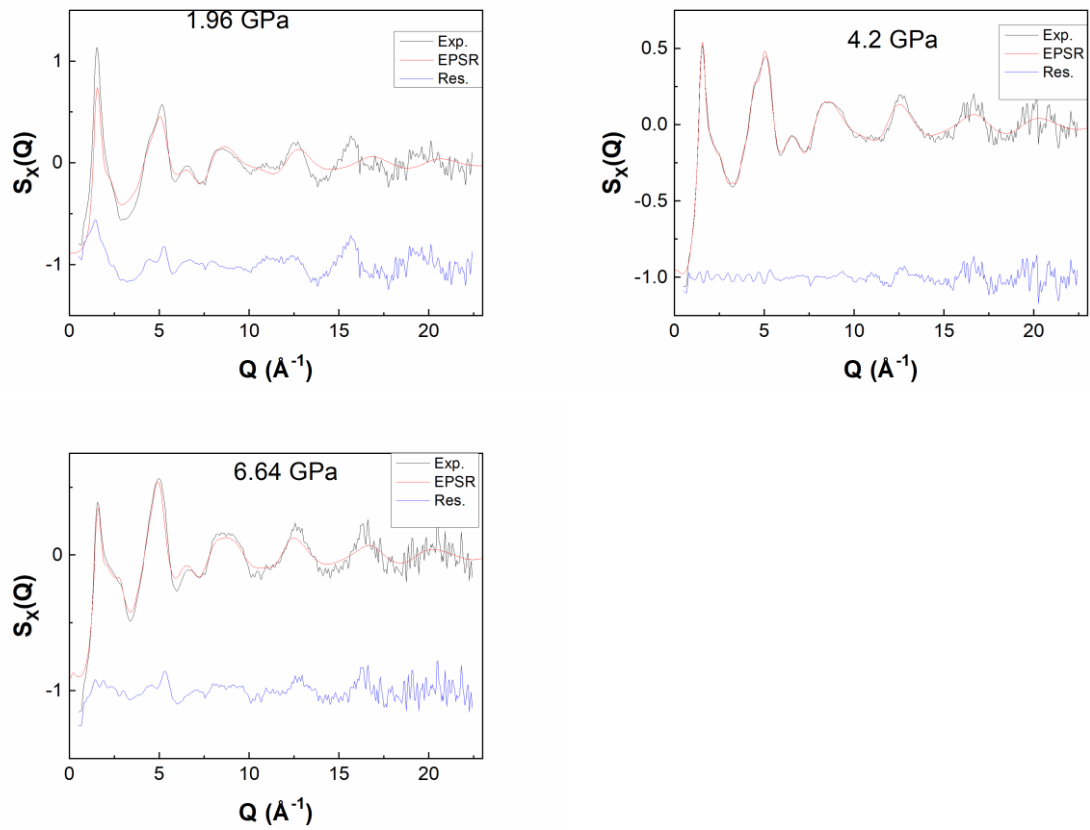
Figure S3. *g*-silica-He composite structure factor $S_X(Q)$ (black). (a) at 1.96 GPa, (b) at 4.2 GPa and (c) at 6.64 GPa; red and blue lines show calculated EPSR model and the difference between calculated and experimental data, respectively.

The comparison of the obtained partial radial distribution functions obtained from the EPSR model with those simulated by molecular dynamics using the CHIK-potential[3] show a near perfect agreement, Figure S4.
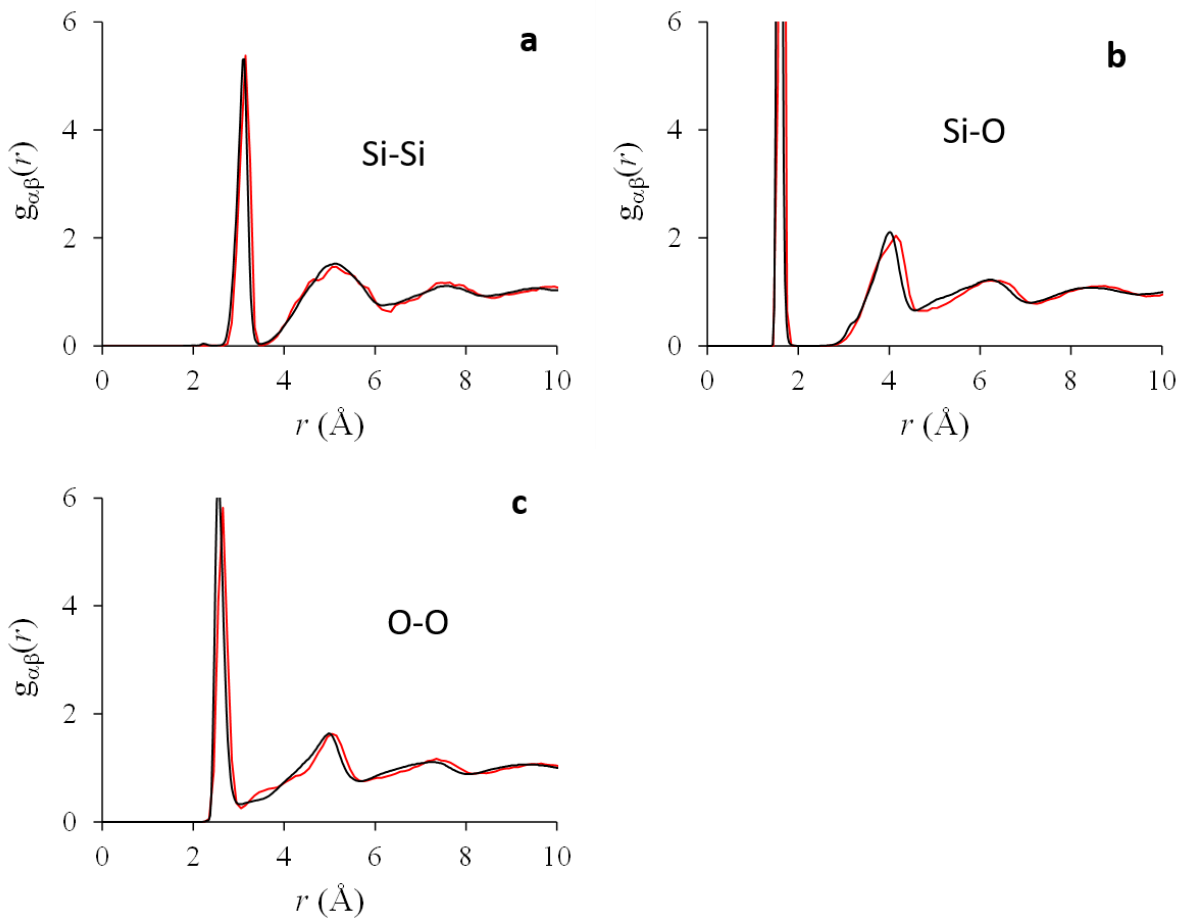
Figure S4. Comparison of the partial radial distribution functions obtained from molecular dynamics (black) and those from EPSR model for *g*-silica at *Patm* (red) (a) Si-Si, (b) Si-O, (c) O-O

In the EPSR structural model, the helium inserted values N_{He}^{P} at each pressure points were fixed to those determined using a poromechanical model[4], Figure S5.
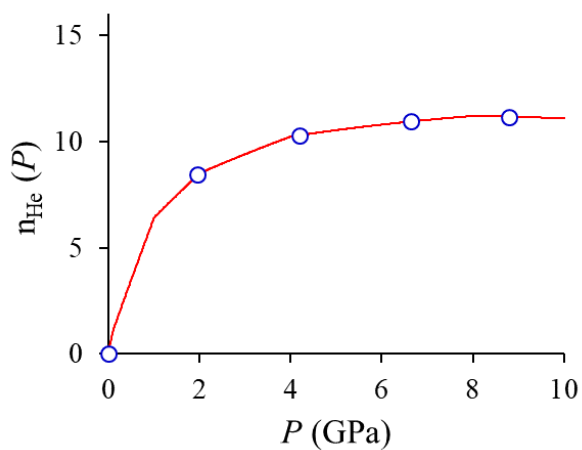
Figure S5. Helium inserted values $N_{He}{}^{P}$ (He-atoms/nm^3) obtained from a poromechanical model[4]. Blue circles are the pressures in this PDF study
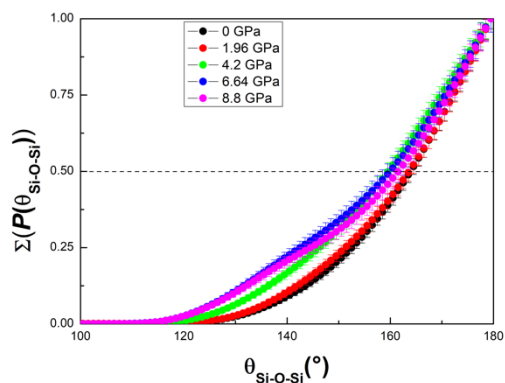

Figure S6. Sum of Si-O-Si bond angle distributions $P(\theta_{Si-O-Si})$. Estimation of the mean bond angle values can be obtained as the sum of these probabilities $P(\theta_{Si-O-Si})$ is equal to 1, so the mean is simply the point where $\Sigma(P(\theta_{Si-O-Si}))$ is 50%.
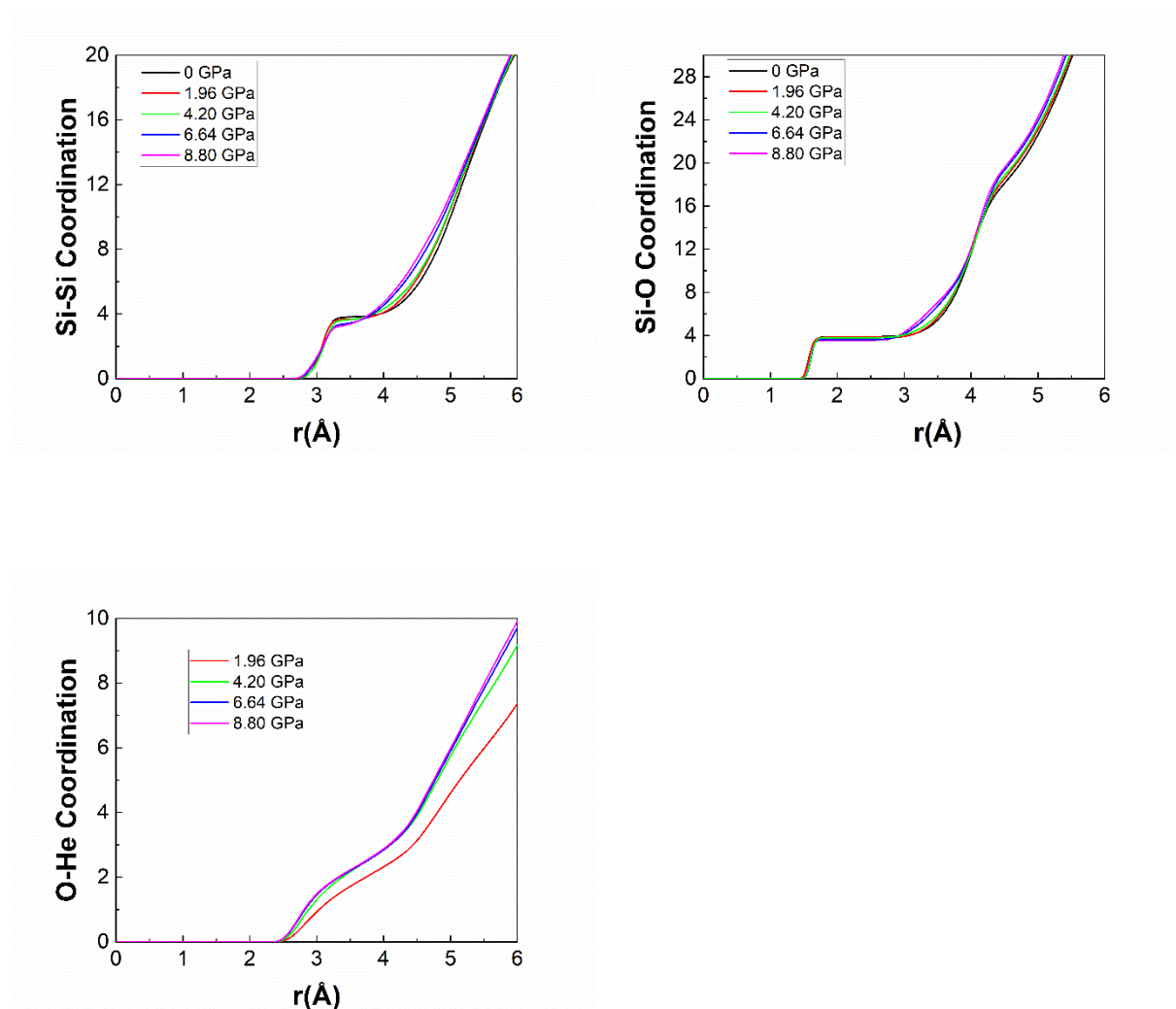
Figure S7. Pressure dependence of Si-Si, Si-O and O-He coordination number determined in this study

As the data in Figure S2 do show some artifacts at high-Q which probably arise from a not-quite perfect background subtraction, the full set of EPSR models were re-run with the reduced Q-range of **15 Å^{-1}** which was applied to the input experimental data. The X-ray structure factor of g-silica obtained at Patm in the diamond cell up to Q = **15 Å^{-1}** along with the structure factor calculated from EPSR model are shown on Figure S8.
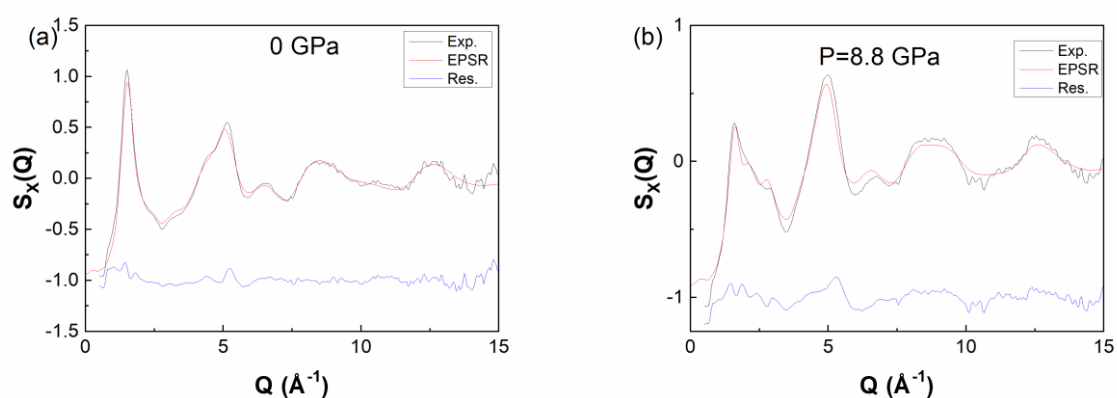
Reduced Q-range (15 Å^{-1}) data and EPSR models:

Figure S8. g-silica-He composite structure factor $S_X(Q)$ (black) limited to **15 Å^{-1}**: (a), at Patm, (b), at 8.8 GPa; red and blue lines show calculated EPSR model and the difference between calculated and experimental data, respectively.

The partial radial distribution functions for Si-Si, Si-O, O-He, as well as the Si-O-Si bond angle distributions obtained from the EPSR model (using a Q-max of 15 Å^{-1} for the experimental data) are shown on Figure S8a-d, respectively and are in perfect agreement with our original results (using a Q-max of 22.5 Å^{-1}). As explained above, this confirms i) that our analysis using EPSR largely ignores these high-Q data with their associated low statistics and ii) completely validate the results of this HP-PDF study.
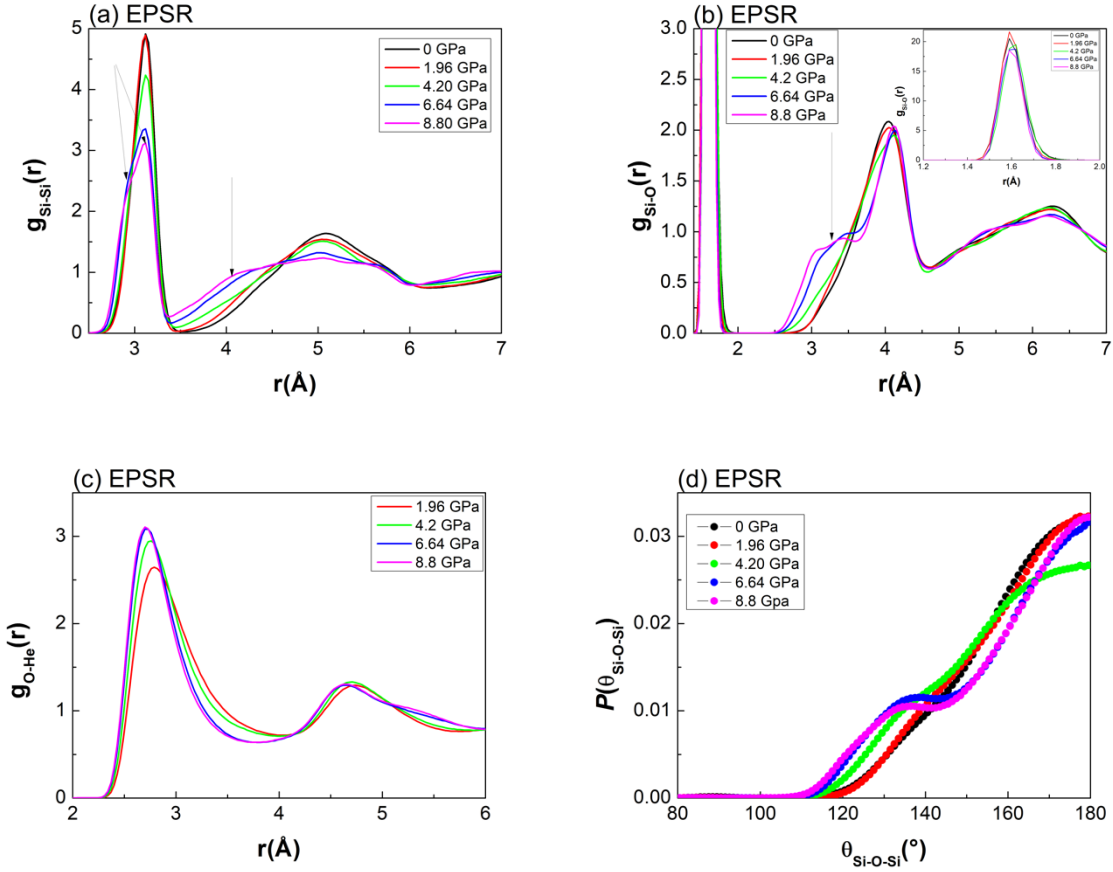
Figure S9. Pressure dependence of the partial radial distribution functions from EPSR model of g-silica-He composite obtained from $S_X(Q)$ limited to **15 Å^{-1}**: (a) $g_{Si-Si}(r)$, (b) $g_{Si-O}(r)$, (c) $g_{O-He}(r)$; arrows either show the appearance of a bi-modal distribution or of a new contribution, and (d) Pressure dependence of Si-O-Si bond angle distribution functions.

High-Pressure Impedance Spectroscopy Study

The Clausius-Mossotti relationship for a-silica-He composite can be written as:

$$3\varepsilon_0 \frac{n^2 - 1}{n^2 + 2} = N_{SiO_2}\alpha_{SiO_2} + N_{He}\alpha_{He}$$

ε_0: permittivity of free space

$n = n^{He}_{a-SiO_2}$: refractive index of the composite

N_{SiO_2}, N_{He}: density values of SiO$_2$ and He

α_{SiO_2}, α_{SiO_2}: polarizability of SiO$_2$ and He

Impedance measurements as a function of frequency 100 kHZ–3 MHz were performed up to 1.6 GPa on g-silica (Suprasil F300) disk of (dimensions) metallized with gold on both faces, Figure S9, with a Rhode Schwartz impedance analyzer on the third stage of a Unipress gas

compressor using either a penetrating (He), i.e. atomic-spring-like, and a non- penetrating medium (gasoline F). The pressure was measured with a manganin gauge.

Figure S10. *g*-silica disk used for impedance measurements

AUTHOR INFORMATION

Corresponding Author

* *Jérôme Rouquette* - ICGM, Univ Montpellier, CNRS, ENSCM, Montpellier, France ; https://orcid.org/0000-0002-6880-1715

Email : Jerome.Rouquette@umontpellier.fr

***Daniel T. Bowron** - ISIS Facility, Rutherford Appleton Laboratory, Harwell Campus, Didcot, OX11 0QX, UK

; https://orcid.org/0000-0002-4557-1929

Email : daniel.bowron@stfc.ac.uk

***David A. Keen** - ISIS Facility, Rutherford Appleton Laboratory, Harwell Campus, Didcot, OX11 0QX, UK

https://orcid.org/0000-0003-0376-2767

Email : david.keen@stfc.ac.uk

Authors

Mathieu Kint - L2C, Univ Montpellier, CNRS, Montpellier, France
Email : mathieu.kint@hotmail.fr

Coralie Weigel - L2C, Univ Montpellier, CNRS, Montpellier, France

Email : Coralie.Weigel@umontpellier.fr

Benoit Ruffle *- L2C, Univ Montpellier, CNRS, Montpellier, France*

Email : Benoit.ruffle@umontpellier.fr

Leszek Konczewicz *- L2C, Univ Montpellier, CNRS, Montpellier, France ; Institut of High Pressure Physics, Polish Academy of Sciences, Sokołowska 29/37, 01-142 Warsaw, Poland.*

Email : leszek.konczewicz@umontpellier.fr

Sylvie Contreras *- L2C, Univ Montpellier, CNRS, Montpellier, France*

Email : Sylvie.Contreras@umontpellier.fr

Benoit Coasne *- Univ. Grenoble Alpes, CNRS, LIPhy, 38000 Grenoble, France*; https://orcid.org/0000-0002-3933-9744

Email : benoit.coasne@univ-grenoble-alpes.fr

Gaston Garbarino *- ESRF, 38000 Grenoble, France*; https://orcid.org/0000-0003-4780-9520

Email : gaston.garbarino@esrf.fr

Mickael Beaudhuin- ICGM, Univ Montpellier, CNRS, ENSCM, Montpellier, France

Email : Mickael.Beaudhuin@umontpellier.fr

Julien Haines - ICGM, Univ Montpellier, CNRS, ENSCM, Montpellier, *France ; https://orcid.org/0000-0002-7030-3213*

Email : Julien.Haines@umontpellier.fr

1   **Mao, H. K., Xu, J. & Bell, P. M. CALIBRATION OF THE RUBY PRESSURE GAUGE TO 800-KBAR UNDER QUASI-HYDROSTATIC CONDITIONS. *Journal of Geophysical Research-Solid Earth and Planets* 91, 4673-4676, doi:10.1029/JB091iB05p04673 (1986).**

2   **Soper, A. K. & Barney, E. R. Extracting the pair distribution function from white-beam X-ray total scattering data. *J. Appl. Crystallogr.* 44, 714-726, doi:10.1107/s0021889811021455 (2011).**

3   **Carre, A., Horbach, J., Ispas, S. & Kob, W. New fitting scheme to obtain effective potential from Car-Parrinello molecular-dynamics simulations: Application to silica. *Epl* 82, doi:10.1209/0295-5075/82/17001 (2008).**

4   **Coasne, B. et al. Poroelastic Theory Applied to the Adsorption-Induced Deformation of Vitreous Silica. *J Phys Chem B* 118, 14519-14525, doi:10.1021/jp5094383 (2014).**